AGU PUBLICATIONS

Water Resources Research

RESEARCH ARTICLE
10.1002/2016WR019464

Key Points:
- A novel approximate methodology that considers both 3-D flow patterns and differential sediment mobility as mechanisms for the self-maintenance of pool-riffle sequences
- Application of the methodology to a pool-riffle sequence on a real stream
- Analysis of different dominant mechanisms for self-maintenance in two contiguous pool-riffle units

Correspondence to:
J. F. Rodríguez,
jose.rodriguez@newcastle.edu.au

Citation:
Bayat, E., J. F. Rodríguez, P. M. Saco, G. A. M. de Almeida, E. Vahidi, and M. H. García (2017), A tale of two riffles: Using multidimensional, multifractional, time-varying sediment transport to assess self-maintenance in pool-riffle sequences, *Water Resour. Res.*, *53*, doi:10.1002/2016WR019464.

Received 7 JUL 2016
Accepted 14 FEB 2017
Accepted article online 18 FEB 2017

A tale of two riffles: Using multidimensional, multifractional, time-varying sediment transport to assess self-maintenance in pool-riffle sequences

Esmaeel Bayat[1], José F. Rodríguez[1], Patricia M. Saco[1], Gustavo A. M. de Almeida[2], Elham Vahidi[1], and Marcelo H. García[3]

[1]Civil, Surveying and Environmental Engineering, The University of Newcastle, New South Wales, Australia, [2]Civil Engineering, Engineering and the Environment, University of Southampton, Southampton, UK, [3]Civil and Environmental Engineering, University of Illinois at Urbana-Champaign, Urbana, IL, USA

Abstract Pool-riffle sequences play a central role in providing habitat diversity conditions both in terms of flow and substrate in gravel bed streams. Understanding their capacity to self-maintain has been the focus of research for many years, starting with the velocity reversal hypothesis. This hypothesis relied only on cross sectional averaged flow information, but its limited success prompted extensions of the hypothesis and alternative explanations for self-maintenance. Significant advances beyond the velocity reversal hypothesis have been achieved by incorporating more information either on flow or sediment transport characteristics. However, this has been done in a compartmentalized way, with studies either focusing on one or the other aspect. This work bridges the gap between these two aspects by using an approximate methodology that combines observed characteristic stage-dependent 3-D flow patterns with time-varying cross sectional information on bed shear stresses, sediment distribution, and sediment bed changes during a 1 year record of continuous discharges from a real stream. This methodology allows us to track the behavior of different sediment size fractions along flow streamlines over time and identify self-maintenance conditions due to the combined effect of both flow multidimensionality and sediment transport. We apply this approximate methodology to two contiguous pools and riffles and demonstrate that, unexpectedly, they may rely on different mechanisms for self-maintenance due to differences in geometry and sediment size distribution. We also demonstrate that our methodology is potentially overarching and integrative of previous partial approaches based on flow multidimensionality or sediment transport, which tend to underestimate the occurrence of self-maintenance.

1. Introduction

Pool-riffle (PR) sequences are one of the most common geomorphological features in gravel bed streams, and play a central role in providing habitat diversity conditions both in terms of flow and substrate [*Emery et al*., 2003]. Because of these features, the addition of artificial PR sequences is a widespread practice in restoration projects [*Newbury and Gaboury*, 1993; *Purcell et al*., 2002; *Emery et al*., 2003; *Wade et al*., 2002; *Rhoads et al*., 2008, 2011; *Walther and Whiles*, 2008; *Whiteway et al*., 2010; *Schwartz et al*., 2015]. Ensuring the long-term stability of PR sequences is a key factor when designing these artificial structures, and looking at natural PR sequences and their capacity to self-maintain can provide valuable insight in that regard.

A number of physical mechanisms and theories have been proposed to explain the observed dynamic stability of natural PR sequences, starting with the velocity reversal hypothesis [*Gilbert*, 1914; *Keller*, 1971]. According to this hypothesis, the difference in geometry between pools and riffles induces a shift in maximum near-bed velocities from the riffles, where they occur during most flow conditions, to the pools during high flows. This velocity shift allows for the removal of the sediment previously deposited in pools during low to medium flows. Accordingly, a ratio of cross sectional averaged near-bed velocities $V_p/V_r > 1$ (subindices p and r denote pool and riffle, respectively) indicates "reversal" conditions, and is used to infer self-maintenance of the PR sequence over the long term. The occurrence of reversal conditions has been investigated using averaged near-bed velocity, or its associated averaged bed shear stress in several studies based on field and laboratory observations, as well as through data from numerical simulations. While some

research supported the theory [*Keller*, 1971; *Jackson and Beschta*, 1982; *Keller and Florsheim*, 1993], several other studies either reported the total absence of reversal or the presence of reversal conditions only in particular pools and riffles of a sequence [*Bhowmik and Demissie*, 1982; *Carling*, 1991; *Clifford and Richards*, 1992; *Clifford*, 1993; *Sear*, 1996; *Carling and Wood*, 1994; *Thompson et al*., 1996, 1999; *Booker et al*., 2001; *Cao et al*., 2003; *Caamaño et al*., 2009]. It is now widely accepted that the velocity reversal hypothesis alone cannot explain self-maintenance in all PR sequences [see for example, *Thompson*, 2011, and references therein].

To address this question on the stability of PR sequences and the inconsistent observation of velocity reversal conditions, alternative or complementary explanations for self-maintenance have been proposed and tested. Most of them have focussed on either multidimensional (2-D or 3-D) flow features [*Booker et al*., 2001; *MacWilliams et al*., 2006; *MacVicar and Roy*, 2007a,b; *Caamaño et al*., 2009, 2012; *Thompson*, 2011; *Rodríguez et al*., 2013; *MacVicar and Best*, 2013; *MacVicar and Obach*, 2015; *Strom et al*., 2016; *Thompson et al*., 1996, 1999] or sediment transport characteristics [*Clifford*, 1993; *Sear*, 1996; *Cui et al*., 2008; *MacVicar and Roy*, 2011; *Milan*, 2013; *de Almeida and Rodríguez*, 2011, 2012; *Hodge et al*., 2013; *Chartrand et al*., 2015].

The idea behind the incorporation of a multidimensional flow analysis is that characteristic flow patterns not captured by the averaged reversal concept may contribute to self-maintenance [*Thompson et al*., 1999; *Booker et al*., 2001; *MacWilliams et al*., 2006; *Harrison and Keller*, 2007; *Thompson and Wohl*, 2009]. For example, *Thompson et al*. [1996, 1999] identified in laboratory experiments the presence of a jet of local high velocities in the pool center, which was generated by a recirculating eddy produced by a forced constriction (an obstacle) at the head of the pool. They argued that the formation of the jet provided a mechanism for preventing deposition at the pool. Although less evident, jets or zones of flow concentration produced by lateral flow convergence/divergence were also identified in several studies of—more commonly occurring—unforced PR sequences using 2-D and 3-D numerical models [*Booker et al*., 2001; *Caamaño et al*., 2012; *MacWilliams et al*., 2006]. These studies reported high velocity zones and associated bed shear stresses, occurring typically in a narrow region of the pool away from the deepest depths, which supports the idea of sediment being routed around and away from the pool center, and therefore preventing deposition. These patterns were stronger for low to medium flows, but tended to decay for higher flows [*MacWilliams et al*., 2006]. Similarly, 3-D measurements by *Rodríguez et al*. [2013] in a laboratory PR sequence showed areas of flow concentration at the pool, with a different concentration pattern for different flow discharges. Some of these flow concentration and routing features were also observed by *Strom et al*. [2016], who used 2-D hydrodynamic simulations to track the spatial dynamics of high-velocity areas (denoted as peak velocity patches) over a wide range of steady state discharges. They concluded that only for discharges substantially above bankfull the high-velocity areas can shift to the pools.

Even though the physical insight gained from the description of flow patterns presented above allowed for the inference of sediment transport patterns (typically using the bed shear stress as a proxy), it did not include specific quantitative predictions of sediment erosion, deposition, and transport. Such sediment processes are related to grain size, packing arrangements, and mobility, and have also been investigated as additional mechanisms for complementing the velocity reversal hypothesis [*Sear*, 1996; *Milan*, 2013; *Vetter*, 2011; *Hodge et al*., 2013; *de Almeida and Rodríguez*, 2011, 2012; *Bayat et al*., 2014]. Evaluation of sedimentological differences between pools and riffles indicates that pool surface sediments are dominated by finer, loosely interacting and unstable particles, whereas riffle surface sediments are coarser, tightly interacting, and more stable [*Sear*, 1996]. Both friction angle and critical shear stress are higher at riffles than at pools and, therefore, sediment transport rates in pools increase with discharge more rapidly than in riffles [*Sear*, 1996]. *Hodge et al*. [2013] used field estimations of sediment grain size, exposure, pivoting angle, and resistance to lift to determine mobility conditions in a PR sequence. By combining differential mobility with typical bankfull flow conditions predicted via a 2-D numerical model, they showed that pool sediment was more likely to be transported than the sediment in the riffles despite experiencing lower shear stresses. *de Almeida and Rodríguez* [2011, 2012] arrived at a similar conclusion when applying a 1-D morphodynamic model comprising fractional sediment transport, unsteady flow, bed deformation, and bed sediment sorting to a real stream. They reported a number of events (typically below bankfull flow) in which sediment transport at the pools was higher than at the riffles, even though bed shear stresses were lower than at the riffles. Those events not only contributed significantly to the overall self-maintenance of the PR sequence but also helped explain PR sequence formation from an initially plane bed with unsorted sediment. As a formal extension of the velocity reversal concept, they used the ratio of cross sectional averaged bed load

sediment transport $Qs_p/Qs_r > 1$ (subindices p and r denoting pool and riffle, respectively) to identify self-maintenance conditions.

As explained above, significant advances in understanding PR self-maintenance beyond the velocity reversal hypothesis have been achieved by incorporating more information either on flow or sediment transport characteristics. However, this has been done in a compartmentalized way, with studies either focusing on one aspect or the other. Bridging that gap is not easy, as combining all identified factors contributing to self-maintenance would require either measuring or modeling unsteady multidimensional flow and sediment transport for different size fractions over a movable and continuously evolving sediment bed at the scale of a PR sequence, a task virtually impossible with current computational and/or instrumental capabilities. Instead, we use here an approximate methodology that combines observed characteristic stage-dependent 3-D flow patterns with time-varying cross sectional information on bed shear stresses, sediment distribution, and sediment bed changes obtained using simulations on a real PR sequence. This methodology allows us to track the behavior of different sediment size fractions along flow streamlines over time and identify self-maintenance conditions due to the combined effect of both flow multidimensionality and sediment transport.

Our objective is to analyze the extent to which each of these mechanisms (multidimensional flow and multifractional sediment transport) contribute to the overall self-maintenance of PR sequences and to identify whether different mechanisms may be prevalent under different conditions that can occur in a real stream. In order to do that, we apply our methodology to follow the evolution of two different PR units in the same river reach during a 1 year record of continuous discharges.

2. Methods

2.1. Estimation of Cross Sectional Averaged Bed Shear Stresses and Sediment Size Distributions

For our analysis we will focus on a reach of the Bear Creek, Arkansas, United States, a gravel bed river with a well-defined and stable PR sequence [*Reuter et al*., 2003]. The reach has a longitudinal slope of 0.2%, a width between 30 and 40 m, a bankfull depth between 5 and 7 m and a bed sediment ($D_{50} = 29.5$ mm and $D_{90} = 50$ mm using the pebble-count method) mostly composed by gravel but with some sand and cobble as well. Morphodynamic changes of the PR sequence in response to an annual series of discharges were modeled by *de Almeida and Rodríguez* [2011, 2012] for the period June 2001 to June 2002 using a 1-D unsteady flow-sediment-bed elevation model. The model used by *de Almeida and Rodríguez* [2011, 2012] solved the Saint-Venant 1-D unsteady flow equations coupled with the fractional sediment transport formulation of *Wilcock and Crowe* [2003] and *Hirano* [1971] equation for grain size distribution changes in the active layer and Exner's law for bed level modifications. Their 1 year simulation of the Bear Creek bed evolution over time clearly showed the effects of grain size distribution on the PR self-maintenance and displayed a very good agreement with measured data. Another important finding from this work was the dominant role of stream width variations on pool and riffle location and bed form size [*de Almeida and Rodríguez*, 2012].

Of the three PR units of the Bear Creek studied by *de Almeida and Rodríguez* [2011] we focus only on PR1 and PR2, as PR3 is influenced by backwater effects from a downstream junction and displays a very particular behavior. Figures 1 and 2 show the most important characteristics of the Bear Creek, including the location and the cross sections of the selected pools and riffles, the longitudinal profile of the reach (Figure 1) and the time series of discharges over the year of simulation (Figure 2).

We use results from the simulations of *de Almeida and Rodríguez* [2011] to derive from the discharge time series of Figure 2 cross sectional averaged values of bed shear stresses τ at the pools and the riffles of PR1 and PR2. Values of τ are determined from the cross sectional averaged values of downstream velocity U, hydraulic radius R and D_{90}, as follows:

$$\tau = \rho C_f U^2 \tag{1}$$

where ρ is the water density and C_f is a friction factor that needs to be estimated from resistance relations. C_f can be computed using Keulegan's law [*Chaudhry*, 2008]:

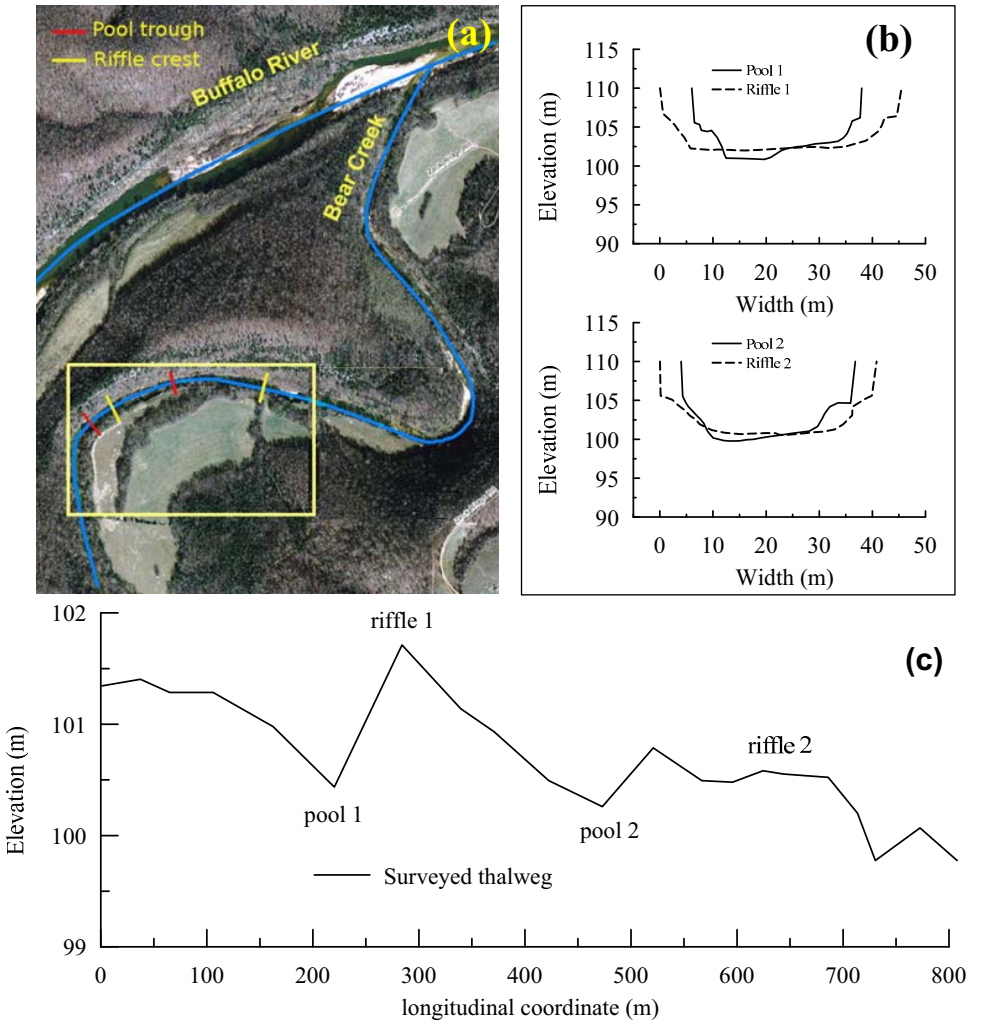

Figure 1. Main characteristics of the Bear Creek used in this study: (a) satellite image showing the reach location (35°59′37.46″N, 92°41′53.92″W), (b) representative pool-riffle cross sections, and (c) longitudinal bed profile with locations of pools and riffles (modified from *de Almeida and Rodríguez* [2011]).

$$C_f^{-1/2} = \frac{U}{u_*} = \frac{1}{\kappa} Ln\left(\frac{11R}{k_s}\right) \tag{2}$$

with u_* *being the shear velocity,* κ *is the von Karman constant* ($\kappa = 0.41$ *adopted here) and* k_s *is the roughness height approximated using* D_{90} *as:*

$$k_s = 2D_{90} \tag{3}$$

2.2. Estimation of Bed Shear Stress Transverse Distributions and Near-Bed Streamlines

In order to incorporate the effects of flow multidimensionality in our methodology, we use detailed 3-D flow data obtained in a laboratory PR sequence by *Rodríguez et al*. [2004, 2013]. The sequence consisted of three pools and three riffles on a 1 m wide straight channel with a slope of 0.25%. As with natural sequences, pools were deeper and narrower than riffles. The effective pool width varied between 0.6 and 0.8 of the riffle width depending of flow conditions, and the distance between consecutive pools (or riffles) was about five times the riffle width. The bed was made out of crushed stone chips ($D_{50} = 5.7$ mm, $D_{90} = 10$ mm), which provided the same fully rough bed conditions that would be expected in a natural PR sequence. Two geometric configurations typically found in streams were considered, one with pools close to one of the banks in an alternating pattern (alternate configuration) and the other one with pools located in the center of the channel (centered configuration).

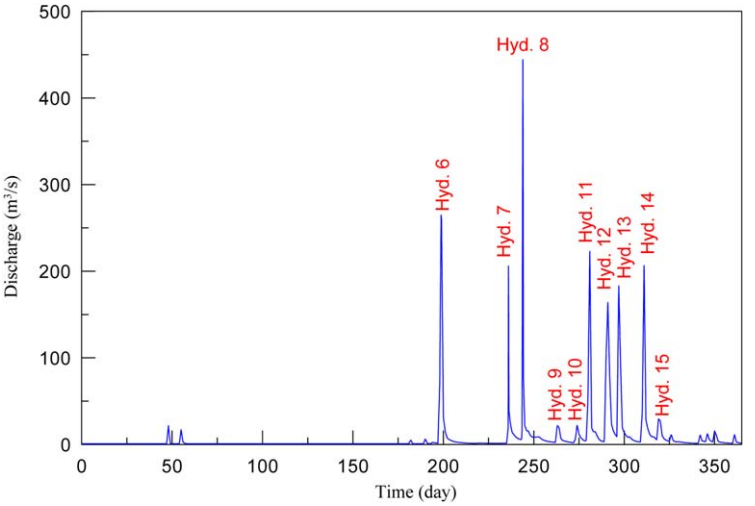

Figure 2. Discharge time series of Bear Creek for the period June 2001 to June 2002, including hydrograph numbers (modified from *de Almeida and Rodríguez* [2011]). Number of days in the horizontal axis counted from 1 June 2001.

Even though these data strictly correspond to a setup that has different characteristics than the Bear Creek pools and riffles, both situations present notable geometric and flow similarities when the variables are normalized using the stream width b as a length scale. Table 1 shows that reach characteristics like longitudinal slope and nondimensional bankfull depth h/b and bankfull discharge $Q/(b^{2.5}g^{0.5})$, as well as PR features like ratio of pool width over riffle width b_p/b_r, nondimensional distance between riffle and pool $(x_r - x_p)/b$ and nondimensional depth from riffle crest to pool trough $(z_r - z_p)/b$ of the laboratory model are very close to the Bear Creek data. In defining the previous variables, we have used x as the longitudinal distance, z as the bed elevation from an arbitrary datum, and subindices p and r to denote pool and riffle locations, respectively.

It must be noted that roughness conditions in the laboratory model were different to the ones in Bear Creek, as is typically the case when comparing laboratory and field setups. However, the effects of these differences on 3-D flow patterns are expected to be minor because they do not produce substantial alterations to flow turbulence and secondary circulation. Table 1 shows values of both the dimensionless roughness k_sU_*/ν *and of the relative roughness* k_s/h, *where* k_s *is estimated for comparison purposes as 2* D_{90}, U_* is an average shear velocity over the PR unit and ν is the kinematic viscosity. The table shows that even though the laboratory dimensionless roughness is smaller than the one for Bear Creek, it is still well above 70 so it generates the same fully rough boundary conditions at the bed [*Nezu and Nakagawa*, 1993]. It also shows that the laboratory relative roughness is larger than in the Bear Creek, but still within a range that does not interfere with secondary flow patterns generated by geometry and turbulence anisotropy [*Rodríguez and García*, 2008; Rodríguez et al., *2013*]. The 3-D flow patterns of the alternate and centered laboratory PR configurations are consistent with patterns in real streams reaches with mild curvature [*Dietrich and Whiting*, 1989; *Whiting and Dietrich*, 1991; *MacWilliams et al*., 2006] and straight [*Thompson*, 1986; *Rhoads et al*., 2008], respectively. Having similar secondary flow patterns in the laboratory and the field is important as secondary flow generates variations in wall shear stress [*Rodríguez and García*, 2008; *Rodríguez et al*., 2013; *MacWilliams et al*., 2006] that will influence local sediment transport. Since PR2 is on a straight reach and its pool location is close the center of the cross section we use the centered PR configuration to describe the 3-D flow patterns. PR1 is downstream of a bend exit and its pool is located closer to the outer bank of the bend, so we use the alternate PR configuration flow patterns in this case. Even though PR1 is located downstream of the exit of a mild curvature bend, residual secondary circulation from the bend may affect the flow at the pool, so our results for PR1 must be considered with caution. However, *de Almeida and Rodríguez* [2011] results showed that the overall morphodynamics of PR1 was driven primarily by width differences between the pool and the riffle and was not greatly affected by the upstream bend curvature.

Table 1. Comparison Between Most Relevant Variables in Laboratory Experiments and Numerical Simulations

Variable	Laboratory Model	Bear Creek PR1 and PR2
$b(m)$	1	30–40
Slope	0.0025	0.002
h/b	0.1–0.2	<0.23
$Q/(b^{2.5}g^{0.5})$	0.015–0.035	0.013–0.026
$(x_p - x_r)/b$	2.7	2–5
$(z_p - z_r)/b$	0.075	0.03–0.05
b_p/b_r	0.85	0.7
ksU^*/ν	1180	4000–18,000
ks/h	0.1	0.01–0.028

The 3-D velocity laboratory data were collected for two representative discharges, which can be described as intermediate and high flow. The intermediate flow experiment captured the typical low to medium flow behavior of PR sequences with the topography exerting a strong control on the longitudinal water surface profile, while the high flow represented near bankfull conditions when the PR topography gets drowned and works more as a large roughness element [*Rodríguez et al*., 2013]. The experimental data included 3-D velocities measured using a down-looking ADV on a dense grid (grid spacing in the vertical and transverse directions Δz and Δy between 1/10 and 1/20 of depth h and width b, respectively) at five locations: upstream riffle, pool entrance, pool center, pool exit, and downstream riffle. Figures 3 and 4 show the measurements at the pool center and the downstream riffle cross sections for the alternate and the centered configuration, respectively, where the fine spatial resolution of the measurement grid can be observed. The density of measurements allowed for reconstruction of the entire 3-D flow field and was used to determine bed shear stresses over the uneven topography of the PR sequence. Bed shear stresses were obtained by applying the law of the wall to reconstructed velocity profiles perpendicular to the bed surface [*Rodríguez and García*, 2008; *Rodríguez et al*., 2013] and then nondimensionalized with the cross sectional average value (Figures 3 and 4).

In addition to the spatially distributed bed shear stress information, near-bed flow directions are required to estimate directions of bed shear stresses and the associated sediment routing through pools and riffles. We used the high-resolution velocity data provided by the 3-D flow experiments at the five cross sections (upstream pool, pool entrance, pool center, pool exit, and downstream riffle) to calculate the near-bed streamlines over the entire PR by time-integration of water particle velocities and tracking the positions of those particles close to the bed [*Gorrick and Rodríguez*, 2012]. This method required velocity information on a regular and very fine grid, which was obtained by linearly interpolating the data into a fine three-dimensional grid. Originally the centered PR configuration only had data over one-half of the cross sections, so it was extended over the entire cross sections assuming central symmetry before implementing the interpolation procedure. From these fine grids, 17 equispaced near-bed streamlines at the downstream riffles were backtracked into the pools and continued all the way to the upstream riffles.

2.3. Estimation of Self-Maintenance Indices Based on Sediment Transport

Following *de Almeida and Rodríguez* [2011] we use the sediment transport reversal concept to assess self-maintenance. We calculate instantaneous values of Qs at the pools (Qs_p) and the downstream riffles (Qs_r) based on bed shear stress and grain size information and determine sediment transport reversal conditions ($Qs_p/Qs_r > 1$) at PR1 and PR2 over the period June 2001 to June 2002. Both the bed shear stress (from equations (1) and (2)) and the sediment size distribution time series are obtained using the 1-D model of *de Almeida and Rodríguez* [2011].

Using the fractional sediment transport formula of *Wilcock and Crowe* [2003] we can incorporate the grain size information into our computations. *Wilcock and Crowe* [2003] consider the total bed load transport of a mixture Qs as the integration of the bed load transport per unit width of each size fraction q_{si}, where i is an index to denote each fraction F_i of diameter D_i. Dimensionless parameters W_i^* and φ represent, respectively, the bed load transport and the relative shear stress for the size i fraction and are related through:

$$W_i^* = \begin{cases} 0.002\phi^{7.5} & \phi < 1.35 \\ 14\left(1-\dfrac{0.894}{\phi^{0.5}}\right)^{4.5} & \phi \geq 1.35 \end{cases} \tag{4}$$

The dimensionless parameters are defined as:

$$W_i^* = \frac{(s-1)gq_{si}}{F_i u_*^3} \tag{5}$$

$$\phi = \frac{\tau}{\tau_{ri}} \tag{6}$$

where s is the ratio of sediment to water density, g is the gravitational acceleration, $u_* = (\tau/\rho)^{1/2}$ *is the shear velocity, and* τ_{ri} *is the reference shear stress for each individual size.* τ_{ri} *can be obtained using:*

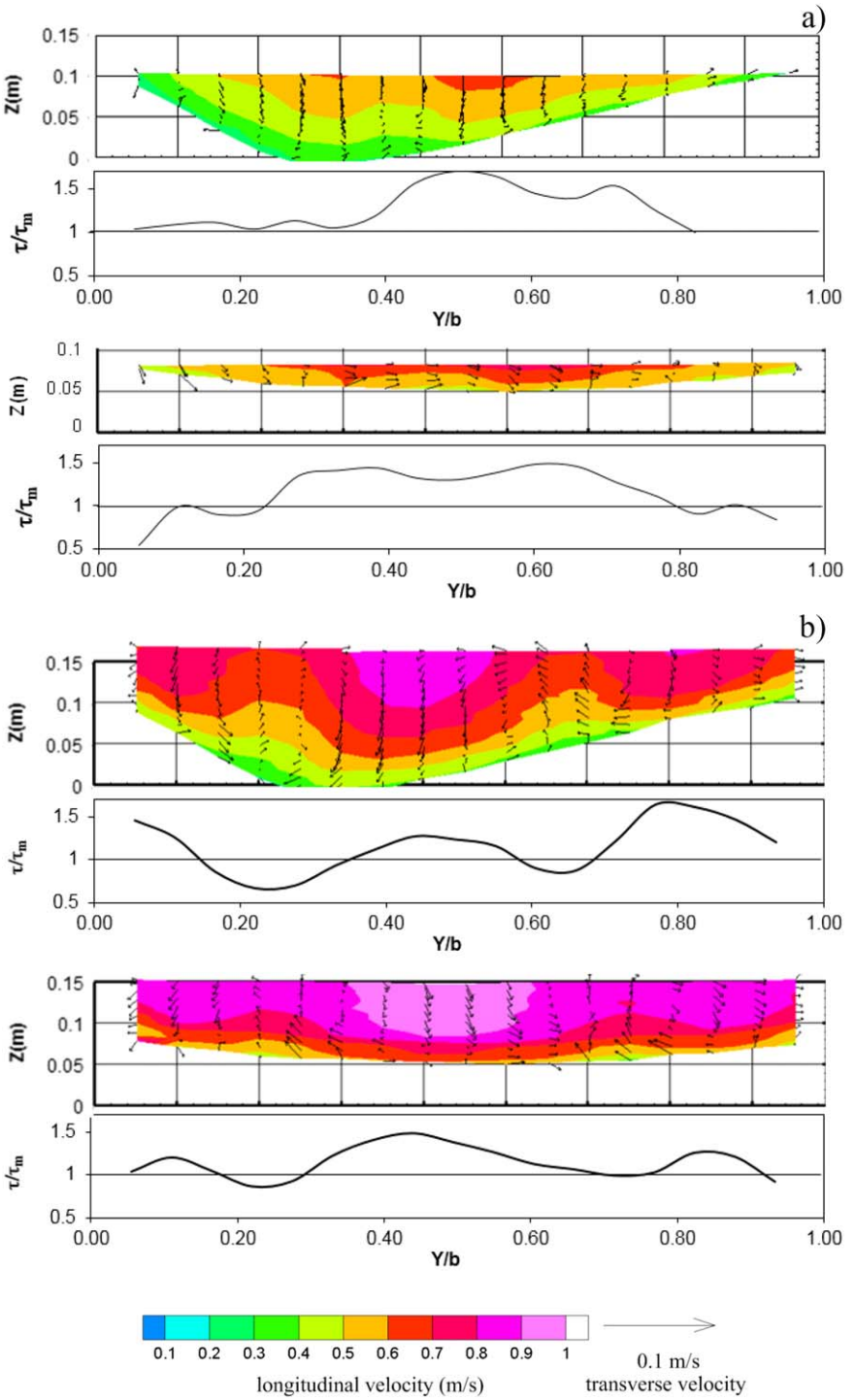

Figure 3. 3-D velocity and shear stress distributions at the alternate pool center and downstream riffle in the laboratory for (a) intermediate flow and (b) high flow. τ is the local shear stress, τ_m is the average cross sectional shear stress, z is the vertical distance from the pool lowest point, b is the width of the channel, and y is the transverse distance from left bank (modified from *Rodríguez et al.* [2004] with permission from ASCE).

$$\tau_{ri} = \tau_{rsm}\left(\frac{D_i}{D_{sm}}\right)^c \tag{7}$$

where τ_{rsm} is the value of τ_{ri} that corresponds to the mean size of the bed D_{sm} and the exponent c is given by:

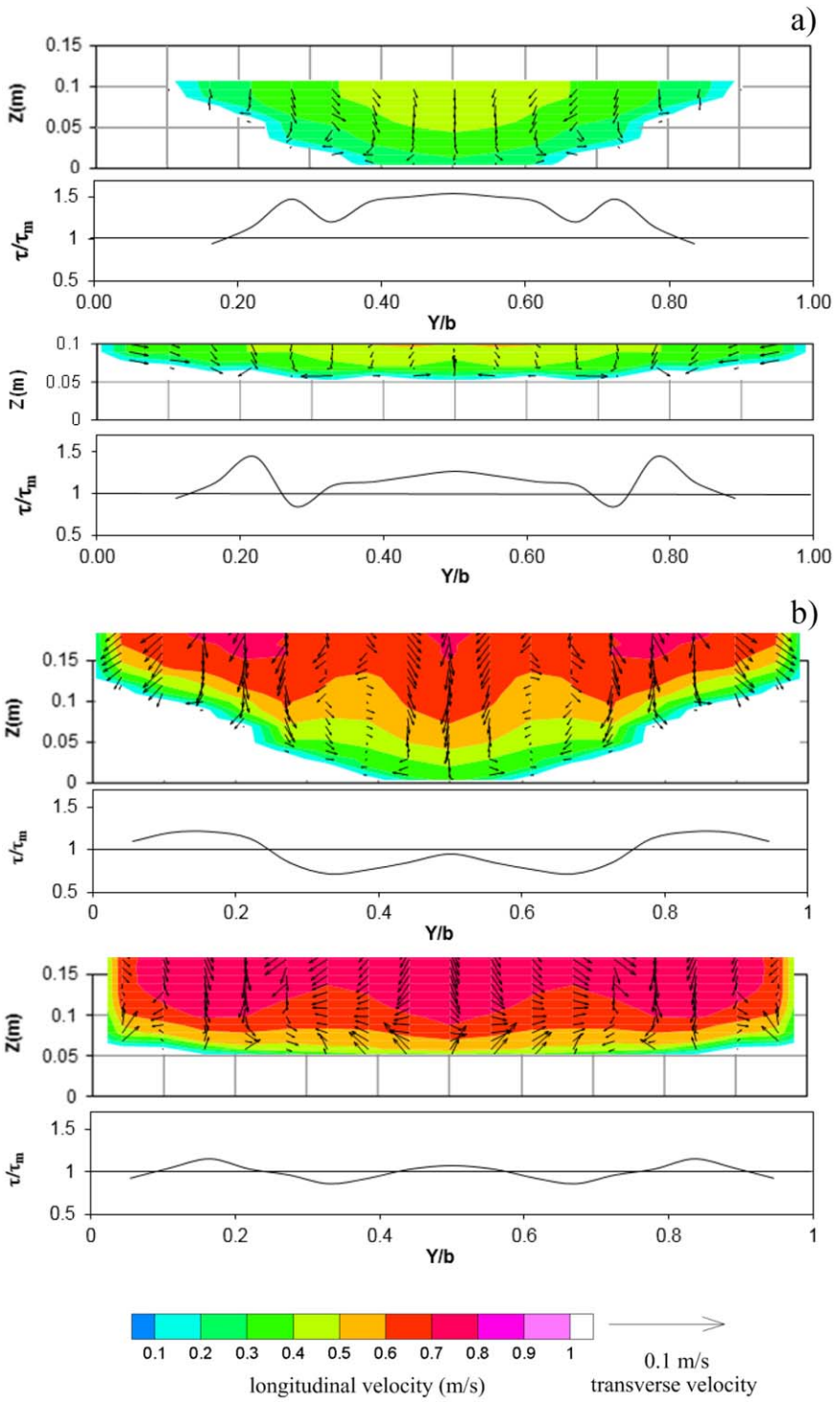

Figure 4. 3-D velocity and shear stress distributions at the centered pool center and downstream riffle in the laboratory for (a) intermediate flow and (b) high flow (modified from *Rodríguez et al.* [2013]). τ is the local shear stress, τ_m is the average cross sectional shear stress, z is the vertical distance from the pool lowest point, b is the width of the channel, and y is the transverse distance from left bank.

$$c=\begin{cases} 0.12 & \frac{D_i}{D_{sm}}<1 \\ \dfrac{0.67}{1+\exp\left(1.5-\frac{D_i}{D_{sm}}\right)} & \frac{D_i}{D_{sm}}\geq 1 \end{cases} \quad (8)$$

τ_{rsm} depends on the full particles size distribution in the bed, and can be expressed as a function of the sand fraction in the mixture F_s:

$$\tau_{rsm}=(s-1)\rho g D_{sm}[0.021+0.015\exp(-20F_s)] \quad (9)$$

Eight size fractions are used to represent the Bear Creek bed sediment [*Reuter et al*., 2003] with the following values of D_i (mm): 0.6, 1.1, 5.6, 22.6, 45.2, 90.5, 181.0, and 362.0. Since the size distribution of the bed is continuously changing as part of the morphodynamic evolution of the reach, the data from *Reuter et al*. [2003] constitute only a snapshot at a particular time. In order to incorporate the time varying sediment composition, we use the model of *de Almeida and Rodríguez* [2011] (which incorporates *Reuter et al*. [2003] data as an initial condition) to obtain time series of each sediment fraction at the pools and the riffles of PR1 and PR2 for the period June 2001 to June 2002.

We then estimate local values of shear stress and sediment size fractions from the cross sectional averaged values of the morphodynamic simulations by applying the dimensionless transverse distributions of bed shear stress from the laboratory measurements. In the absence of detailed field information, we also use the same distribution of bed shear stresses to modify the cross sectional averaged sediment size distributions. The assumption of a linear relation between sediment sizes and bed shear stresses is a good approximation for gravel-bed rivers where sediment is close to mobility conditions [*Dietrich and Whiting*, 1989; *Whiting and Dietrich*, 1991] and is often used either to model [*de Almeida and Rodríguez*, 2011, 2012] or infer [*MacWilliams et al*., 2006] morphodynamic processes. Using local values of shear stress and sediment size distributions we track sediment being transported through PR1 and PR2 on each of the 17 streamlines. We calculate for each streamline the instantaneous local values of Qs_p and Qs_r and determine 17 instantaneous local values of Qs_p/Qs_r at each PR. Reversal conditions on streamlines can then be analyzed individually (i.e., $Qs_p/Qs_r>1$ in one streamline) or integrated spatially considering simultaneous reversal conditions in more than one streamline.

For comparison purposes, we also compute cross sectional averaged values of sediment transport reversal using cross sectional averaged bed shear stresses obtained using equations (1–3) into equations (4–10).

3. Results

Estimation of the fractional sediment transport used in our methodology required the knowledge of the sediment size distribution at different locations in PR1 and PR2. Hourly values of each of the eight fractions used during the 1 year simulation were extracted from the model results of *de Almeida and Rodríguez* [2011] and combined to construct sediment size distribution curves at the pools and the riffles. Figure 5

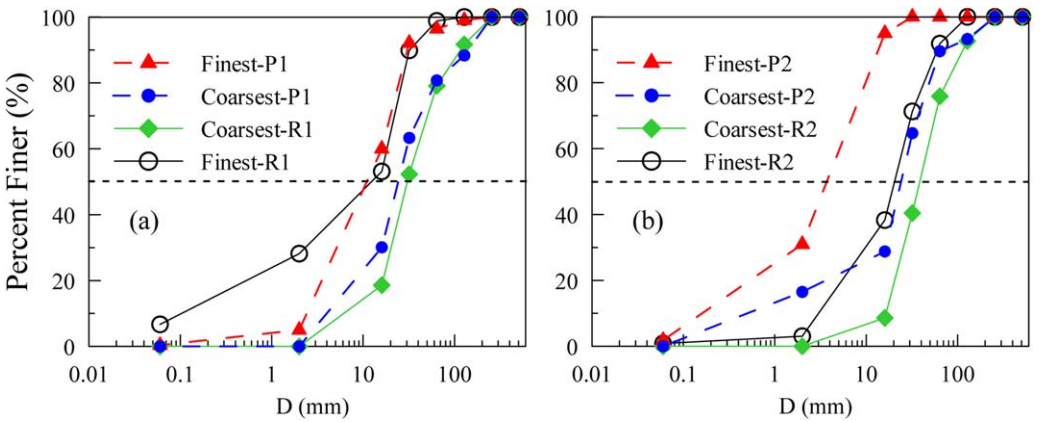

Figure 5. Envelope range of sediment size distributions: (a) PR1 and (b) PR2.

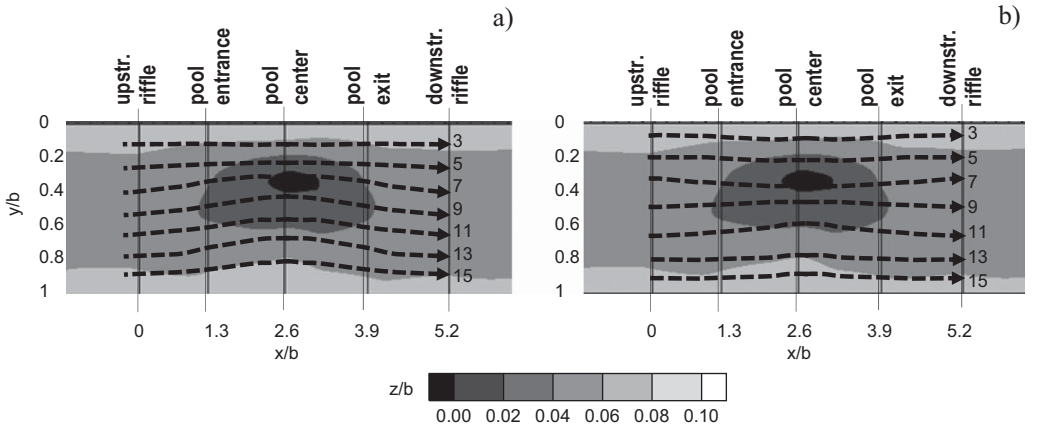

Figure 6. Local streamlines of near-bed velocity in the alternate pool-riffle: (a) intermediate flow and (b) high flow. Only some of the 17 calculated streamlines are shown for clarity with their corresponding number. *x* is the streamwise distance from the upstream riffle.

shows the envelope (finer and coarser) of all cross sectional averaged size distributions obtained at the pool and the riffle of PR1 (labeled as P1 and R1, respectively) and the pool and the riffle of PR2 (labeled as P2 and R2, respectively). This figure shows that PR1 has in general coarser sediment than PR2, and also that the distributions in P1 and R1 are less differentiated than P2 and R2. PR2 clearly shows coarser material at the riffle than at the pool, while in PR1 the size distributions in the pool and the riffle considerably overlap. Even though the size distributions varied over the year of simulation, the pattern of Figure 5 was maintained.

The intermediate and high flow laboratory measurements used to represent the 3-D effects not only displayed different shear stress distributions but also specific near-bed streamline patterns. Figure 6 and 7 show the near-bed streamline patterns obtained for the two flow conditions overlaid to the bed contour lines for the alternate and the centered configurations, respectively. The intermediate flow patterns (Figures 6a and 7a) are affected by the geometry of the pool and show contraction at the pool induced by the narrower and deeper cross section and also a curvature effect in Figure 6a due to the off-center position of the pool in the alternate configuration. The streamline patterns change for the high flow conditions (Figures 6b and 7b), with a more localized contraction effect close to the pools than during intermediate flows.

As explained in section 1, by incorporating a 3-D flow distribution we expect to see an increase in reversal occurrences compared to reversals detected using cross sectional averaged information because reversal may occur in only part of the cross section. We computed sediment transport reversal indices Qs_p/Qs_r for the entire year of simulations at PR1 and PR2 both using cross sectional averaged shear stresses and the

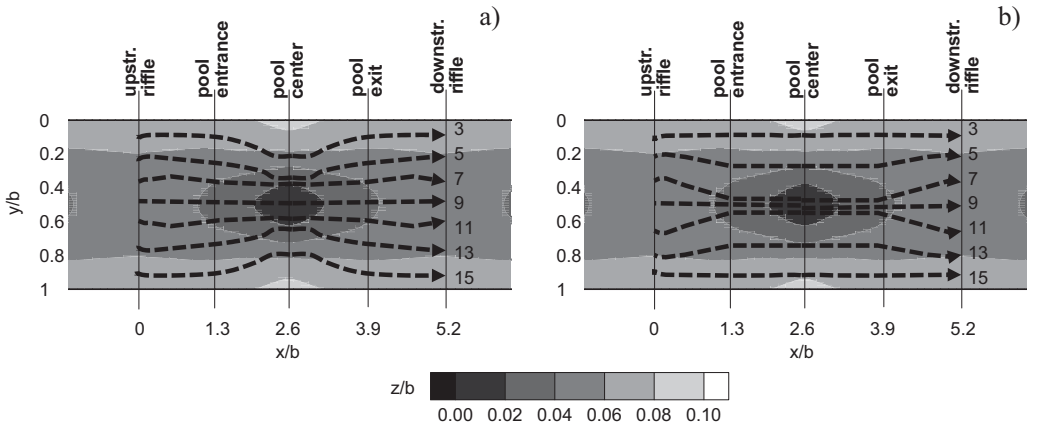

Figure 7. Local streamlines of near-bed velocity in the centered pool-riffle: (a) intermediate flow and (b) high flow. Only some of the 17 calculated streamlines are shown for clarity with their corresponding number. *x* is the streamwise distance from the upstream riffle.

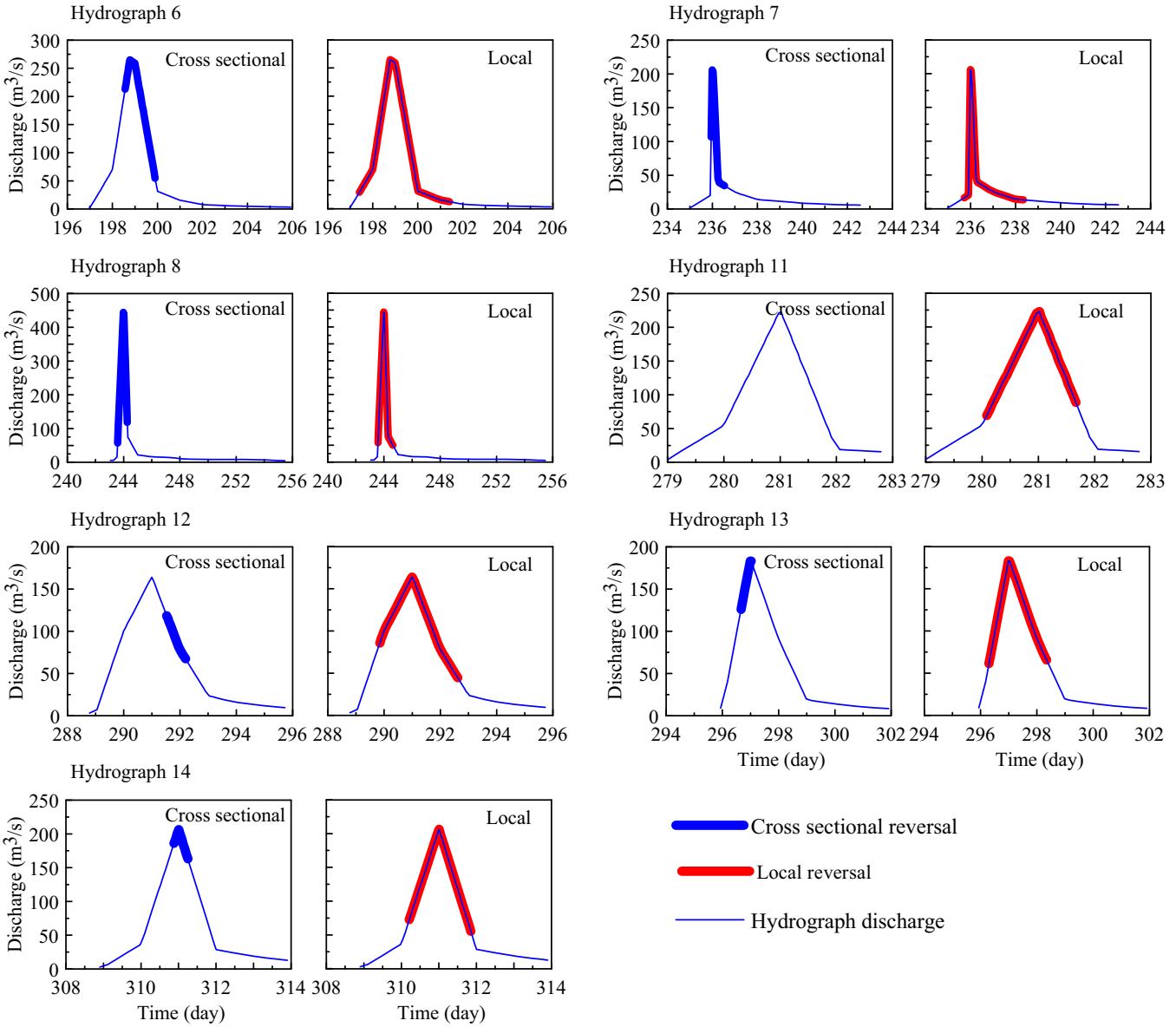

Figure 8. Sediment transport reversal events in PR1 computed using both cross sectional and local (streamline) information. Number of days in the horizontal axis counted from 1 June 2001.

streamline, local values to identify reversal conditions. As mentioned before, the streamlines and bed shear stresses of the alternate PR configuration of Figures 4 and 6 are used to determine 3-D flow patterns in PR1, whereas the corresponding information of the centered configuration (Figures 5 and 7) is associated to PR2. In each case, we classified the discharges of the stream into below and above bankfull flow events, using the approximate bankfull discharge of 170 m^3/s as the transition between the two stages [*de Almeida and Rodríguez*, 2011], and we assigned the intermediate flow patterns to below bankfull flows and the high flow patterns to the above bankfull conditions. Figures 8 and 9 show the results for PR1 and PR2 during all hydrographs in which sediment transport reversal was detected. PR1 displayed cross sectional averaged reversal conditions in six hydrographs, but the incorporation of local information helped identify one more hydrograph (number 11) with reversal conditions (Figure 8). Also, in hydrographs where both cross sectional averaged and local reversal occurred, local reversal conditions started earlier on the raising limb, and finished later on the receding limb. When considering all hydrographs, local reversal conditions occurred during a total of 307 h compared to 102 h of cross sectional averaged reversal conditions. A similar situation was observed in PR2, where the 3-D streamline methodology helped identify reversal conditions for three

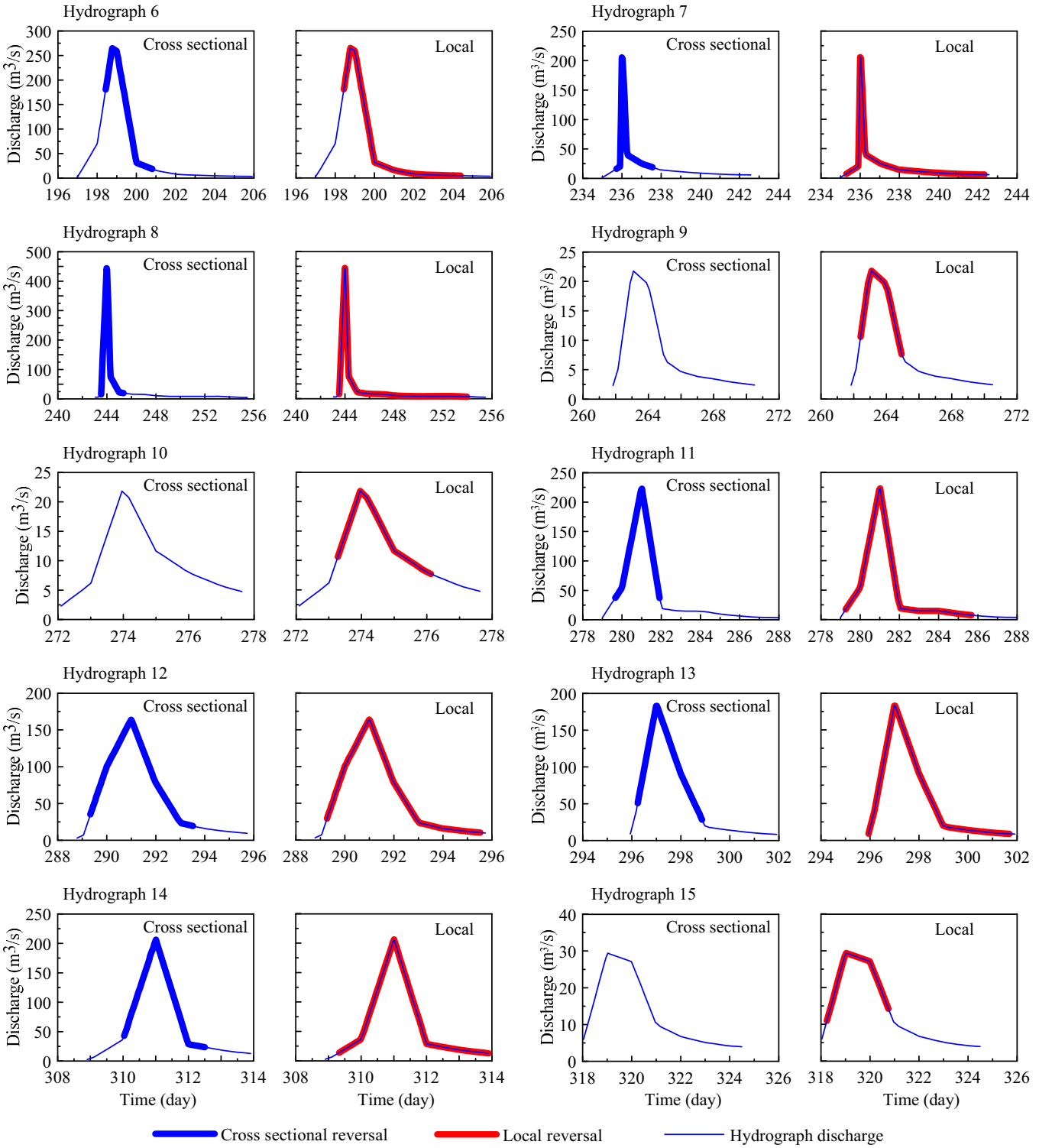

Figure 9. Sediment transport reversal events in PR2 computed using both cross sectional and local (streamline) information. The number of days in the horizontal axis are counted from 1 June 2001.

additional hydrographs (number 9, 10, and 15) than the cross sectional averaged calculations (Figure 9). Total time of reversal conditions increased from 341 to 557 h when the 3-D flow effects were incorporated.

Local reversal conditions did not necessarily occur simultaneously in all streamlines, as each one of them was experiencing different conditions in terms of bed shear stress and sediment size distribution. Figure 10

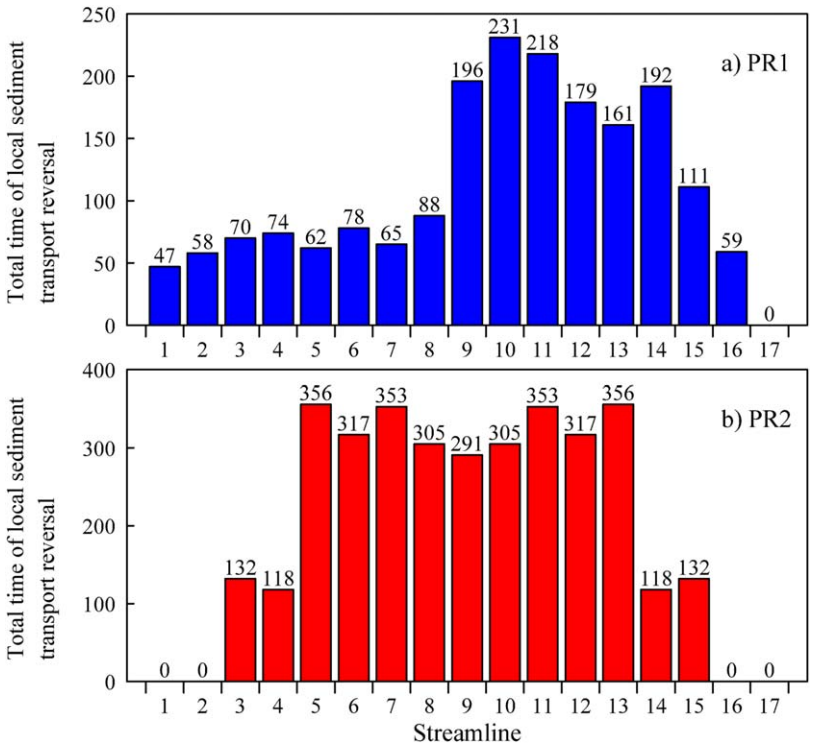

Figure 10. Total time of local sediment transport reversal in different streamlines for (a) PR1 and (b) PR2. Numbers on the horizontal axis represent streamline numbers.

shows the total number of hourly episodes for which each streamline experienced sediment transport reversal conditions in PR1 and PR2. This figure clearly shows that in PR1 the streamlines located on the opposite side to the deeper area of the pool (number 9–14) present more frequent reversal conditions, while in PR2 the majority of the reversal episodes occur in the nine central streamlines (number 5–13).In PR2, the maximum number of reversal episodes did not occur on the streamlines at the center of the cross section but slightly to the sides (streamlines number 5–7 and 11–13).

The previous results show that PR1 and PR2 have different dynamics, with PR2 experiencing reversal conditions more frequently than PR1. This characteristic behavior can be associated with differences in flow three-dimensionality and/or differences in sediment composition, as both factors affect sediment transport. In order to further explore this aspect, we analyze the relation between the sediment transport reversal index Qs_p/Qs_r and the shear stress reversal index τ_p/τ_r in PR1 and PR2 considering both cross sectional averaged and local (streamline) reversal indices (Figure 11). We perform the calculations every 1 h and we refer to each point as an event.

Figures 11a and 11b are divided into four quadrants defined by the lines of $Qs_p/Qs_r = 1$ and $\tau_p/\tau_r = 1$. Events in quadrants III and IV display no sediment transport reversal ($Qs_p/Qs_r < 1$) and promote riffle erosion and pool deposition. Events in quadrants I ($Qs_p/Qs_r > 1$ and $\tau_p/\tau_r > 1$) and II ($Qs_p/Qs_r > 1$ and $\tau_p/\tau_r < 1$) both indicate sediment transport reversal, but only in the first case the sediment transport reversal can be associated with differences in flow conditions that generate shear stress reversal. Quadrant I events can in principle be explained by the traditional velocity reversal hypothesis and the complementary theories of sediment routing based on flow information only. Quadrant II events require finer sediment at the pools than at the riffles, as flow mechanisms alone are not enough to produce self-maintenance. When cross sectional values are considered (Figure 11a) PR1 experiences less quadrant II events than PR2, so differences in bed sediment in pool and riffle are less important for self-maintenance. The same trend is observed when local values of shear stresses and sediment transport are considered (Figure 11b), even though the spread of the data makes this behavior less evident. In fact, curve fits to the data of Figures 11a and 11b have essentially the same mathematical formulation. For the cross sectional averaged values (Figure 11a), the lines of best fit for PR1 and PR2 are, respectively:

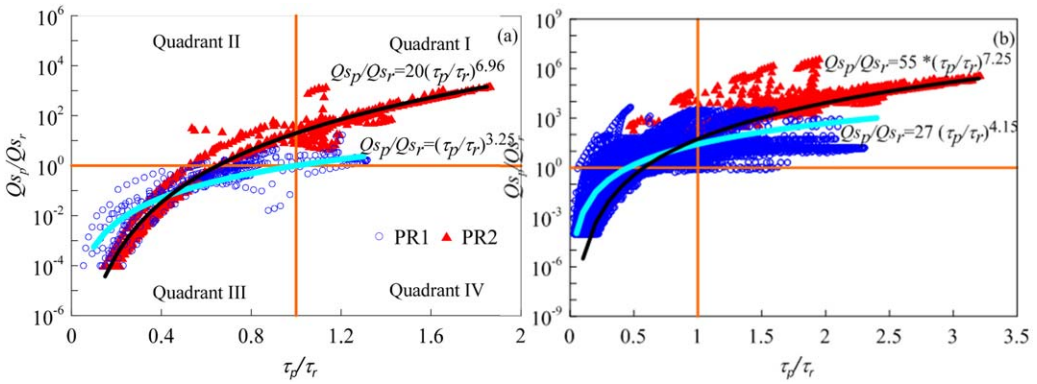

Figure 11. Relationship between flow reversal (τ_p/τ_r) and sediment transport reversal (Qs_p/Qs_r) indices in PR1 and PR2: (a) cross sectional formulation using 1-D information and (b) local formulation using 3-D information.

$$\frac{Qs_p}{Qs_r} = 1\left(\frac{\tau_p}{\tau_r}\right)^{3.25} \tag{9}$$

$$\frac{Qs_p}{Qs_r} = 20\left(\frac{\tau_p}{\tau_r}\right)^{6.96} \tag{10}$$

When local values are considered (Figure 11b), the best fit lines for data on PR1 and PR2 are:

$$\frac{Qs_p}{Qs_r} = 27\left(\frac{\tau_p}{\tau_r}\right)^{4.15} \tag{11}$$

$$\frac{Qs_p}{Qs_r} = 55\left(\frac{\tau_p}{\tau_r}\right)^{7.25} \tag{12}$$

4. Discussion

Even though PR1 and PR2 are both stable pools and riffles that are located in close proximity within the Bear Creek, they present significant differences in geometric and sediment characteristics. Compared to PR2, PR1 has a pool that is more constricted and closer to the riffle (Figure 1), and does not have the same degree of differentiation between sediment size at the pool and the riffle (Figure 5). These differences in characteristics drive two contrasting dynamics for self-maintenance that we can explain based on our new approach.

The level of flow contraction at the pools is also different for flows below and above bankfull, which has implications for self-maintenance when combined with the bed shear stress distributions of Figures 3 and 4. The streamlines of Figures 6 and 7 show that flows below bankfull are affected by contraction effects over a wider pool area than flows above bankfull. In addition, below bankfull flows display a concentration of bed shear stresses in the central areas of the pool, unlike above bankfull flows that have noticeable less concentration of bed shear stresses in these areas. This highlights the importance of below bankfull 3-D flow patterns as contributors to self-maintenance, particularly since below bankfull flows are considerably more frequent. Figures 8 and 9 show that only hydrographs 6 and 8 have maximum values well above bankfull discharge, yet most other hydrographs still provide conditions for self-maintenance.

As mentioned in the previous section, the transverse distribution of reversal events displayed in Figure 10 reveals that in PR1 streamlines 9–11 experience reversal conditions more frequently. During below bankfull flows these streamlines are located slightly away from the deepest part of the pool (Figure 7) and over the areas of maximum bed shear stress (Figure 4a). This behavior is consistent with the flow convergence routing hypothesis [*MacWilliams et al.*, 2006], which postulates that sediment is routed around the deepest part of the pool without actually going through it. However, in PR2 we have a different pattern of reversal events with more frequent occurrence in the central part of the cross section (streamlines 5–13) closer to the pool deepest part. Above bankfull conditions are slightly different in both PR1 and PR2, with higher shear

Table 2. Number of Reversal Events Detected Using Different Criteria (Cross Sectional Average Bed Shear Stress Reversal (Average τ_p/τ_r), Local Bed Shear Stress Reversal Along Streamlines (Streamline τ_p/τ_r), Cross Sectional Average Sediment Transport Reversal (Average Qs_p/Qs_r), and Local Sediment Transport Reversal Along Streamlines (Streamline Qs_p/Qs_r) in PR1 and PR2 for Below Bankfull and Above Bankfull Discharges

	PR1			PR2		
Detection Criteria	Below Bankfull	Above Bankfull	Total	Below Bankfull	Above Bankfull	Total
Average τ_p/τ_r	16	38	54	179	68	247
Streamline τ_p/τ_r	159	72	231	395	72	467
Average Qs_p/Qs_r	50	52	102	269	72	341
Streamline Qs_p/Qs_r	235	72	307	485	72	557

stresses affecting other streamlines that are closer to the banks (14 in PR1; 3 and 15 in PR2) and generating increases in reversal frequency in those areas.

Figure 10 also shows that PR1 and PR2 have quite a different behavior in terms of total number of reversal events. More insight can be gained by looking at the relationship between the sediment transport reversal index Qs_p/Qs_r and the shear stress reversal index τ_p/τ_r presented in Figures 11a and 11b. Assuming a typical relationship between Qs and τ of the form $Qs = a\,\tau^d$ it is easy to show that the best fit curve for PR1 in Figure 11a given by equation (9) describes a situation in which both the riffle and the pool have similar values of the coefficients a and d. Since the *Wilcock and Crowe* [2003] sediment transport equation used in this work can be considered to have values of a and d that are dependent on the sediment size distribution, the general behavior described by equation (9) implies that a and d are the same at the pool and the riffle and the sediment size differences between them are not important for the self-maintenance process in PR1. The exponent d of 3.25 of the best fit curve is consistent with low mobility material in the *Wilcock and Crowe* [2003] formula corresponding to the relative shear stress coefficient $\varphi \geq 1.35$ in equation (4).

In contrast, the best fit curves for PR2 given by equation (10) includes amplification factors of 20, which can be associated with differences in sediment size distribution between the pool and the riffle. The exponent of 6.96 corresponds to the middle to upper range given by the *Wilcock and Crowe* [2003] methodology for $\varphi < 1.35$, and indicates a more mobile sediment than in PR1.

Consequently, equations (9) and (10) imply that a key reason for the distinct dynamics of PR1 and PR2 is their differences in sediment size distribution. PR2 has on average a finer sediment size distribution than PR1 and also more marked differences between sediment sizes at the pool and the riffle. This explanation is consistent with the sediment size distributions of Figure 5. Due to these differences the reversal events in PR1 are located mainly in quadrant I of Figure 11a, where the original velocity reversal hypothesis can be used to explain self-maintenance. Reversal events in PR2, on the other hand, are located both in quadrants I and II, a region where the effects of sediment size contributes to the explanation of self-maintenance.

When local flow patterns and sediment distributions are used in the estimation of bed shear stresses and sediment transport (Figure 11b), the data points show a displacement of the reversal events toward quadrants 1 and 2. The trend line equations for PR1 (11) and for PR2 (12) show that PR2 has a more mobile sediment than PR1 as its Qs_p/Qs_r versus τ_p/τ_r relation has a higher exponent. Equation (12) also has a higher amplification factor, which indicates that differences between sediment size in the pool and the riffle are more important in PR2 than in PR1. Compared to Figure 11a, the range of values of Qs_p/Qs_r and τ_p/τ_r in Figure 11b expands considerably, which means that stronger and potentially more severe events of erosion and deposition can occur locally.

The difference in behavior between PR1 and PR2 can also be analyzed in terms of the number of reversal events as presented in Table 2. We compute the number of reversal events using different detection criteria, including: (1) cross sectional average bed shear stress reversal (corresponding to the traditional velocity reversal hypothesis of *Keller* [1971]), (2) local bed shear stress reversal along streamlines (in line with the routing hypothesis of *MacWilliams et al.* [2006]), (3) cross sectional average sediment transport reversal (corresponding to the hypothesis put forward by *de Almeida and Rodríguez* [2011]), and (4) local sediment transport reversal along streamlines as outlined in this work. In general, reversal conditions are present more frequently during below bankfull ($<$170 m^3/s) than during above bankfull flows ($\geq$170 m^3/s), because the bed experiences more below bankfull flows. Table 2 also shows that the detection of PR1 reversal events

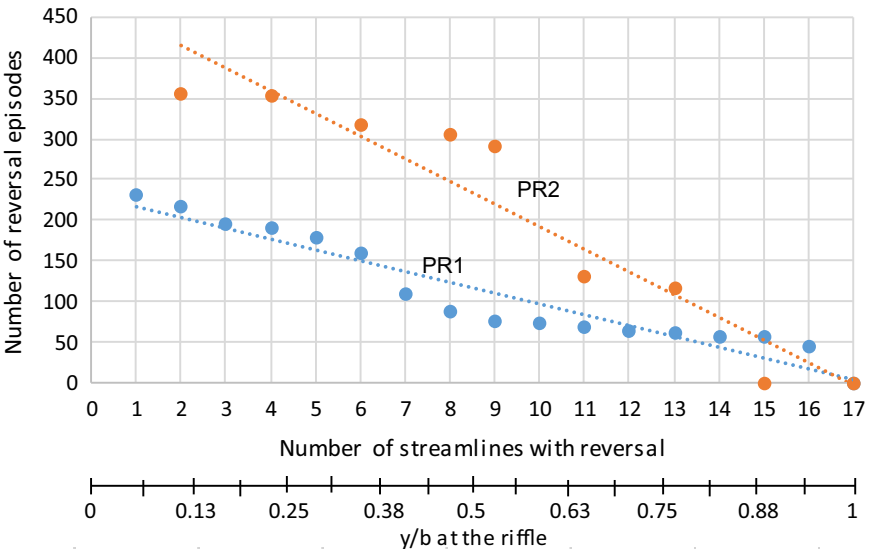

Figure 12. Effect of spatial scale on the number of sediment reversal events detected.

increases substantially when 3-D flow patterns are included (by a factor of four) but does not change when the additional effect of sediment size is considered. In contrast, including 3-D flow patterns increases the detection of reversal conditions in PR2 by a factor of about two and by a similar additional amount when sediment size is incorporated. This different behavior agrees with the previous quadrant analysis and is driven by the contrasting sediment size distributions of PR1 and PR2, with PR2 displaying larger differences in sediment size distributions between the pool and the riffle. Detection of events during above bankfull flows is only marginally affected by the incorporation of 3-D flow effects and unaffected by the consideration of sediment size effects. As already pointed out and based on the streamline patterns of Figure 5, these high flows experience less contraction compared to low flows and thus a more uniform velocity and bed shear stress pattern. The absence of sediment size effects is expected during high flows, as generalized sediment movement during high flows generates a very similar size distribution in pools and riffles.

As pointed out by *Strom et al*. [2016], the size of the spatial domain of analysis affects the identification of reversal conditions. The criteria for detection of reversal events using the streamline method of Table 2 was based on the occurrence of reversal in at least one streamline, which represents a spatial scale of the order of 0.06 of the stream width. In order to assess the effect of the spatial scale of analysis we varied our detection criteria for sediment transport reversal to include more streamlines with simultaneous reversal. The corresponding results are shown in Figure 12, in which we have included in the horizontal axis the minimum number of streamlines affected by reversal and also the minimum proportion of the riffle width over which reversal conditions occur. It can be seen that both PR1 and PR2 still experience a considerable number of reversal events if we modify the detection criteria for reversal to include at least half of the stream width, with the total number of reversals reaching 120 in PR1 and 220 in PR2. This number of episodes represent about 5 and 10 days of reversal conditions for PR1 and PR2 in a year, respectively. More research is needed to establish the minimum temporal and spatial requirements to ensure the self-maintenance of PR sequences, but our results can be used as a guide for the design of artificial self-maintaining PR sequences.

5. Conclusions and Practical Implications for Design

The combined effect of 3-D flow and sediment mobility into the assessment of reversal conditions shows that conditions for self-maintenance may occur far more often (two to four times) than previously thought based on predictions of the traditional velocity reversal hypothesis. Our approximate methodology indicates that self-maintenance conditions can occur for discharges substantially smaller than bankfull discharge, and hydrographs with discharges as low as 1/7 of the bankfull discharge can display local sediment transport reversal conditions because of finer sediment and flow velocity concentration at the pools.

We were able to separate the effects of flow three-dimensionality from the effects of sediment mobility by analyzing local reversal on bed shear stresses. This computation was of interest since sediment differential mobility can vary widely not only between PR sequences in different reaches but also within pools and riffles in the same reach [*Chartrand et al*., 2015]. Furthermore, sediment mobility information is sometimes difficult to obtain and can be substantially modified during hydrographs. According to our findings, flow three dimensionality alone can explain between 70% and 100% of the local reversal events, which supports previous findings by *Booker et al*. [2001], *MacWilliams et al*. [2006], *Caamaño et al*. [2012], and *Strom et al*. [2016] that relied on bed shear stress information to assess self-maintenance.

We also isolated sediment transport effects from flow three-dimensionality by computing reversal of cross sectional averaged values of sediment transport and comparing it with cross sectional averaged bed shear stress reversal. Our results show an increase in self-maintenance events due to sediment effects of between 40% and 100% when compared with the flow processes associated with the original velocity reversal hypothesis, in agreement with results from *de Almeida and Rodríguez* [2011] and *Hodge et al*. [2013].

Our methodology allows us to separate the individual effects of three-dimensional and sediment transport processes, which can be important from a practical point of view in order to assess the predictive capability of simplified assessments of self-maintenance that do not consider all interacting processes. Perhaps more importantly, our results can also be used to analyze the potential different response of individual pools and riffles, like the two pools and riffles of this study.

Even though the two pools and riffles analyzed, PR1 and PR2, are contiguous, they seem to rely on different mechanisms for self-maintenance. Compared to PR2, PR1 has consistently a more similar sediment size distribution in the pool and the riffle and a more constricted pool, so an important mechanism for self-maintenance is the shift of the maximum bed shear stresses toward the pool during hydrographs as stated in the velocity reversal hypothesis. Incorporation of 3-D flow effects significantly increases the number of reversal events, particularly in the central half of the stream width. Sediment size and mobility effects, on the other hand, do not substantially increase the occurrence of reversal events.

In contrast, the self-maintenance of PR2 is heavily influenced by the clear difference in size between the pool and the riffle. Compared to predictions based on the velocity reversal hypothesis, both 3-D flow effects and differential sediment mobility mechanisms increase the number of reversal events by similar amounts.

The different morphodynamic behavior of the two pools and riffles can be represented by simple relations between the sediment transport reversal index Qs_p/Qs_r and the bed shear stress reversal index τ_p/τ_r (equations (9–12)). These equations are consistent with sediment transport theory and their coefficients are likely to be related to sediment mobility and differences in mobility between pool and riffle material. More research on this aspect is needed to clarify whether these equations can be generalized to other PR systems.

Our findings contribute to the understanding of the complex interacting processes affecting the self-maintenance of natural PR sequences. From a practical point of view, our results can be used to select strategies for design of artificial PR sequences or to protect existing ones. Efforts to implement artificial PR sequences in restoration projects have shown, both through field measurements and numerical simulations, that flow within these sequences is highly three dimensional and that serious consideration must be given to the sediment load characteristics [see for example, *Rhoads et al*. [2011]. Two important parameters for design that emerge from our results and previous research are the pool over riffle width (contraction ratio) and the pool over riffle sediment size (mobility ratio). According to our results for PR1, a contraction ratio of 0.6–0.7 is enough to promote self-maintenance even if the mobility ratio is close to 1. In addition, when the mobility ratio is less than 1 self-maintenance conditions are more frequent, as shown by our results for PR2 in which a 0.3 mobility ratio increased the occurrence of self-maintenance events by about 40%.

Another important finding of our research has practical implications for design. The spatial scale analysis performed over PR1 and PR2 in Figure 12 showed that as the area affected by reversal increases the detection of reversal events (or duration of reversal conditions) decreases, as also observed by *Strom et al*. [2016]. This information can be used to select a relevant spatial scale and estimate how often reversal occurs at this particular scale. More research is needed to identify the minimum duration and spatial scale over which reversal conditions are required in order to ensure the long term self-maintenance of the PR sequence, but our results for two stable pools and riffles can be used as a guidance for design.

Acknowledgments
This work has been possible due to funding from the University of Newcastle through two PhD scholarships for E. Bayat and E. Vahidi, and a grant from the Australian Research Council awarded to P.M. Saco (FT140100610). The data used in this study are available upon request from José F. Rodríguez, jose.rodriguez@newcastle.edu.au.

References

Bayat, E., J. F. Rodriguez, G. A. M. de Almeida, and P. M. Saco (2014), Sediment transport, sorting and three-dimensional flow patterns in pool-riffle sequences: Implications for self-maintenance, in *Proceedings of the International Conference on Fluvial Hydraulics, River Flow*, Lausanne, Switzerland, CRC/Balkema, Leiden, The Netherlands, doi:10.1201/b17133-171.

Bhowmik, N. G., and M. Demissie (1982), Bed material sorting in pools and riffles, *J. Hydraul. Div. Am. Soc. Civ. Eng.*, *108*(HY10), 1227–1231.

Booker, D., D. Sear, and A. Payne (2001), Modelling three-dimensional flow structures and patterns of boundary shear stress in a natural pool-riffle sequence, *Earth Surf. Processes Landforms*, *26*, 553–576.

Caamaño, D., P. Goodwin, J. M. Buffington, J. C. Liou, and S. Daley-Laursen (2009), Unifying criterion for the velocity reversal hypothesis in gravel-bed rivers, *J. Hydraul. Eng.*, *135*, 66–70, doi:10.1061/(ASCE)0733-9429(2009)135:1(66).

Caamaño, D., P. Goodwin, and J. Buffington (2012), Flow structure through pool-riffle sequences and a conceptual model for their sustainability in gravel-bed rivers, *River Res. Appl.*, *28*, 377–389, doi:10.1002/rra.1463.

Cao, Z., P. Carling, and R. Oakey (2003), Flow reversal over a natural pool-riffle sequence: A computational study, *Earth Surf. Processes Landforms*, *28*, 689–705, doi:10.1002/esp.466.

Carling, P. (1991), An appraisal of the velocity-reversal hypothesis for stable pool-riffle sequences in the River Severn, England, *Earth Surf. Processes Landforms*, *16*, 19–31, doi:10.1002/esp.3290160104.

Carling, P., and N. Wood (1994), Simulation of flow over pool-riffle topography: A consideration of the velocity reversal hypothesis, *Earth Surf. Processes Landforms*, *19*, 319–332, doi:10.1002/esp.3290190404.

Chartrand, S. M., M. A. Hassan, and V. Radić (2015), Pool-riffle sedimentation and surface texture trends in a gravel bed stream, *Water Resour. Res.*, *51*, 8704–8728, doi:10.1002/2015WR017840.

Chaudhry, M. H. (2008), *Open Channel Flow*, Springer, New York.

Clifford, N. (1993), Differential bed sedimentology and the maintenance of riffle-pool sequences, *Catena*, *20*, 447–468.

Clifford, N. J., and K. Richards (1992), The reversal hypothesis and the maintenance of riffle-pool sequences: A review and field appraisal, in *Lowland Floodplain Rivers: Geomorphological Perspectives*, edited by P. Carling and G. Petts, pp. 43–70, John Wiley, Chichester, U. K.

Cui, Y., J. K. Wooster, J. G. Venditti, S. R. Dusterhoff, W. E. Dietrich, and L. S. Sklar (2008), Simulating sediment transport in a flume with forced pool-riffle morphology: Examinations of two one-dimensional numerical models, *J. Hydraul. Eng.*, *134*, 892–904, doi:10.1061/(ASCE)0733-9429(2008)134%3A7(892).

de Almeida, G. A. M., and J. F. Rodríguez (2012), Spontaneous formation and degradation of pool-riffle morphology and sediment sorting using a simple fractional transport model, *Geophys. Res. Lett.*, *39*, L06407, doi:10.1029/2012GL051059.

de Almeida, G. A. M., and J. F. Rodríguez (2011), Understanding pool-riffle dynamics through continuous morphological simulations, *Water Resour. Res.*, *47*, W01502, doi:10.1029/2010WR009170.

Dietrich, W. E., and P. J. Whiting (1989), Boundary shear stress and sediment transport in river meanders of sand and gravel, in *River Meandering, Water Resources Monograph Series*, vol. 12S, edited by G. P. Ikeda, pp. 1–50, AGU, Washington, D. C.

Emery, J. C., A. M. Gurnell, N. J. Clifford, G. E. Petts, I. P. Morrissey, and P. J. Soar (2003), Classifying the hydraulic performance of riffle-pool bedforms for habitat assessment and river rehabilitation design, *River Res. Appl.*, *22*, 533–549, doi:10.1002/rra.744.

Gilbert, G. K. (1914), The transportation of debris by running water, *U.S. Geol. Surv. Prof. Pap.*, *86*, 263.

Gorrick, S., and J. F. Rodríguez (2012), Sediment dynamics in a sand bed stream with riparian vegetation, *Water Resour. Res.*, *48*, W02505, doi:10.1029/2011WR011030.

Harrison, L. R., and E. A. Keller (2007), Modeling forced pool-riffle hydraulics in a boulder-bed stream, southern California, *Geomorphology*, *83*, 232–248, doi:10.1016/j.geomorph.2006.02.024.

Hirano, M. (1971), River bed degradation with armouring, *Trans. Jpn. Soc. Civ. Eng.*, *3*, 194–195.

Hodge, R. A., D. A. Sear, and J. Leyland (2013), Spatial variations in surface sediment structure in riffle–pool sequences: A preliminary test of the Differential Sediment Entrainment Hypothesis (DSEH), *Earth Surf. Processes Landforms*, *38*, 449–465, doi:10.1002/esp.3290.

Jackson, W., and R. Beschta (1982), A model of two-phase bedload transport in an Oregon coast range stream, *Earth Surf. Processes Landforms*, *7*, 517–527.

Keller, E., and J. L. Florsheim (1993), Velocity-reversal hypothesis: A model approach, *Earth Surf. Processes Landforms*, *18*, 733–740, doi:10.1002/esp.3290180807.

Keller, E. A. (1971), Areal sorting of bed-load material: The hypothesis of velocity reversal, *Geol. Soc. Am. Bull.*, *82*, 753–756, doi:10.1130/0016-7606(1971)82[753:ASOBMT]2.0.CO;2.

MacVicar, B., and J. Best (2013), A flume experiment on the effect of channel width on the perturbation and recovery of flow in straight pools and riffles with smooth boundaries, *J. Geophys. Res. Earth Surf.*, *118*, 1850–1863, doi:10.1002/jgrf.20133.

MacVicar, B., and L. Obach (2015), Shear stress and hydrodynamic recovery over bedforms of different lengths in a straight channel, *J. Hydraul. Eng.*, *141*, 04015025 (1–13), doi:10.1061/(ASCE)HY.1943-7900.0001043.

MacVicar, B., and A. Roy (2007a), Hydrodynamics of a forced riffle pool in a gravel bed river: 1. Mean velocity and turbulence intensity, *Water Resour. Res.*, *43*, W12401, doi:10.1029/2006WR005272.

MacVicar, B., and A. Roy (2007b), Hydrodynamics of a forced riffle pool in a gravel bed river: 2. Scale and structure of coherent turbulent events, *Water Resour. Res.*, *43*, W12402, doi:10.1029/2006WR005274.

MacVicar, B., and A. Roy (2011), Sediment mobility in a forced riffle-pool, *Geomorphology*, *125*, 445–456, doi:10.1016/j.geomorph.2010.10.031.

MacWilliams, M. L., J. M. Wheaton, G. B. Pasternack, R. L. Street, and P. K. Kitanidis (2006), Flow convergence routing hypothesis for pool-riffle maintenance in alluvial rivers, *Water Resour. Res.*, *42*, W10427, doi:10.1029/2005WR004391.

Milan, D. J. (2013), Sediment routing hypothesis for pool-riffle maintenance, *Earth Surf. Processes Landforms*, *38*, 1623–1641, doi:10.1002/esp.3395.

Newbury, R., and M. Gaboury (1993), Exploration and rehabilitation of hydraulic habitats in streams using principles of fluvial behavior, *Freshwater Biol.*, *29*, 195–210, doi:10.1111/j.1365-2427.1993.tb00757.x.

Nezu, I., H. Nakagawa (1993), *Turbulence in Open Channel Flows*, Balkema, Rotterdam, The Netherlands.

Purcell, A. H., C. Friedrich, and V. H. Resh (2002), An assessment of a small urban stream restoration project in northern California, *Restor. Ecol.*, *10*, 685–694, doi:10.1046/j.1526-100X.2002.01049.x.

Reuter, J. M., R. B. Jacobson, and C. M. Elliott (2003), Physical stream habitat dynamics in lower Bear Creek, northern Arkansas, *Biol. Sci. Rep., USGS/BRD/BSR-2003-0002*, 122 pp., U.S. Geol. Surv., Columbia, Mo.

Rhoads, B. L., M. H. Garcia, J. F. Rodriguez, F. Bombardelli, J. D. Abad, and M. Daniels (2008), Methods for evaluating the geomorphological performance of naturalized rivers: Examples from the Chicago metropolitan area, in *Uncertainty in River Restoration*, edited by D. Sears and S. Darby, 209–228, John Wiley, Chichester, U. K., doi:10.1002/9780470867082.ch11.

Rhoads, B. L., F. L. Engel, and J. D. Abad (2011), Pool-riffle design based on geomorphological principles for naturalizing straight channels, in *Stream Restoration in Dynamic Fluvial Systems*, pp. 367–384, AGU, doi:10.1029/2010GM000979.

Rodríguez, J. F., and M. H. García (2008), Laboratory measurements of 3-D flow patterns and turbulence in straight open channels with rough bed, *J. Hydraul. Res.*, *46*, 454–465, doi:10.3826/jhr.2008.2994.

Rodríguez, J. F., F. M. López, C. M. García, and M. H. García (2004), Laboratory experiments on pool-riffle sequences designed to restore channelized low-gradient streams, in *Protection and Restoration of Urban and Rural Streams*, edited by M. Clar et al., 339–348, *Am. Soc. of Civ. Eng.*, Reston, Va., doi:10.1061/40695(2004)34.

Rodríguez, J. F., C. M. García, and M. H. García (2013), Three-dimensional flow in centered pool-riffle sequences, *Water Resour. Res.*, *49*, doi:10.1029/2011WR011789.

Schwartz, J. S., K. J. Neff, F. E. Dworak, and R. R. Woockman (2015), Restoring riffle-pool structure in an incised, straightened urban stream channel using an ecohydraulic modeling approach, *Ecol. Eng.*, *78*, 112–126, doi:10.1016/j.ecoleng.2014.06.002.

Sear, D. (1996), Sediment transport processes in pool-riffle sequences, *Earth Surf. Processes Landforms*, *21*, 241–262.

Strom, M. A., G. B. Pasternack, and J. R. Wyrick (2016), Reenvisioning velocity reversal as a diversity of hydraulic patch behaviors, *Hydrol. Processes*, *30*(13), 2348–2365, doi:10.1002/hyp.10797.

Thompson, A. (1986), Secondary flows and the pool-riffle unit: A case study of the processes of meander development, *Earth Surf. Processes Landforms*, *11*, 631–641, doi:10.1002/esp.3290110606.

Thompson, D., and E. E. Wohl (2009), The linkage between velocity patterns and sediment entrainment in a forced-pool and riffle unit, *Earth Surf. Processes Landforms*, *34*, 177–192, doi:10.1002/esp.1698.

Thompson, D. M. (2011), The velocity-reversal hypothesis revisited, *Prog. Phys. Geogr.*, *35*, 123–132, doi:10.1177/0309133310369921.

Thompson, D. M., E. E. Wohl, and R. D. Jarrett (1996), A revised velocity-reversal and sediment-sorting model for a high-gradient, pool-riffle stream, *Phys. Geogr.*, *17*, 142–156.

Thompson, D. M., E. E. Wohl, and R. D. Jarrett (1999), Velocity reversals and sediment sorting in pools and riffles controlled by channel constrictions, *Geomorphology*, *27*, 229–241.

Vetter, T. (2011), Riffle-pool morphometry and stage-dependant morphodynamics of a large floodplain river (Vereinigte Mulde, Sachsen-Anhalt, Germany), *Earth Surf. Processes Landforms*, *36*, 1647–1657, doi:10.1002/esp.2181.

Wade, R. J., B. L. Rhoads, J. F. Rodriguez, M. Daniels, D. Wilson, E. E. Herricks, F. Bombardelli, M. Garcia, and J. Schwartz (2002), Integrating science and technology to support stream naturalization near Chicago, Illinois, *J. Am. Water Resour. Assoc.*, *38*, 931–944, doi:10.1111/j.1752-1688.2002.tb05535.x.

Walther, D. A., and M. R. Whiles (2008), Macroinvertebrate responses to constructed riffles in the Cache River, Illinois, USA, *Environ. Manage.*, *41*, 516–527, doi:10.1007/s00267-007-9058-2.

Whiteway, S. L., P. M. Biron, A. Zimmermann, O. Venter, and J. W. Grant (2010), Do in-stream restoration structures enhance salmonid abundance? A meta-analysis, *Can. J. Fish. Aquat. Sci.*, *67*, 831–841, doi:10.1139/F10-021.

Whiting, P. J., and W. E. Dietrich (1991), Convective accelerations and boundary shear stress over a channel bar, *Water Resour. Res.*, *27*(5), 783–796, doi:10.1029/91WR00083.

Wilcock, P. R., and J. C. Crowe (2003), Surface-based transport model for mixed-size sediment, *J. Hydraul. Eng.*, *129*, 120–128, doi:10.1061/(ASCE)0733-9429(2003)129:2(120).